Nanoscale

RSC Publishing

PAPER

View Article Online
View Journal | View Issue

Small-scale heat detection using catalytic microengines irradiated by laser†

Cite this: *Nanoscale*, 2013, **5**, 1345

Zhaoqian Liu,[ab] Jinxing Li,[ab] Jiao Wang,[a] Gaoshan Huang,[a] Ran Liu*[b] and Yongfeng Mei*[ab]

Received 29th August 2012
Accepted 26th November 2012

DOI: 10.1039/c2nr32494f

www.rsc.org/nanoscale

We demonstrate a novel approach to modulating the motion speed of catalytic microtubular engines *via* laser irradiation/heating with regard to small-scale heat detection. Laser irradiation on the engines leads to a thermal heating effect and thus enhances the engine speed. During a laser on/off period, the motion behaviour of a microengine can be repeatable and reversible, demonstrating a regulation of motion speeds triggered by laser illumination. Also, the engine velocity exhibits a linear dependence on laser power in various fuel concentrations, which implies an application potential as local heat sensors. Our work may hold great promise in applications such as lab on a chip, micro/nano factories, and environmental detection.

1 Introduction

Autonomous locomotion of micro/nano objects in fluids has attracted a lot of attention for its capacity to efficiently convert diverse energies to motion energy without external fields, and for its potential applications in cargo transportation, drug delivery for biomedical therapy, and in powering smart nano machines/factories. Inspired by a self-propelled plate designed by Whitesides,[1] intensive efforts have been devoted to the synthesis of micro/nano motors featuring efficient conversion of chemical fuels to kinetic energy. The propulsion of chemically powered micro/nano engines is generally initiated by the chemical reaction on the liquid–engine interface. Though there is still no consensus on the direct dynamics of motion, the mechanism of "bubble propulsion" has been widely accepted in tubular engines, such as oxygen bubble propulsion induced by the catalytic decomposition of hydrogen peroxide on a Pt segment,[2–6] and hydrogen bubble propulsion by oxidization of an inner Zn surface in an acidic medium.[7]

So far, small man-made machines in various structures such as rods, spheres and tubes have been developed and investigated.[5,8–15] Unlike rod/sphere based catalytic motors, autonomous tubular microengines produce oxygen bubbles from the inner catalytic surface of Pt and accumulate the bubbles in the tubular cavity, giving rise to more efficient bubble propulsion after expelling the evolved microbubbles from the larger openings of the tubular structures. Therefore, diverse methodologies, *e.g.* the template-assisted technique,[16] rolled-up nanotechnology,[2,5,6] and the electrochemical layering approach,[17] have been adopted to fabricate micro/nano tubular jet engines.

Great improvements in the speed and motion control of catalytic microjet engines have recently been achieved. The propulsion speed of catalytic microengines is enhanced by carefully designing the composition and structure of the tubes,[17] while motion control of these self-propelled engines relies on external fields, comprising magnetic or electric fields, which can be used to steer the moving direction of micro/nano motors simply by adding a functional layer between the outer and inner surfaces.[4,18–21] In addition to these methods, external stimuli such as electrochemical conditions,[22,23] elevated temperatures,[14,24] or light[25,26] can also affect chemical reactions and thus control the motion behaviour of the jet engines.

The approach to regulating propulsion speed (chemical reaction rate) by modulating the surrounding temperature shows that the catalytic engines are sensitive to the temperature of the nearby medium, indicating another promising application of these catalytic engines as a localized heat sensor. To date, diverse applications of micro/nano motors have been envisaged and demonstrated, and are mainly focused on biomedical therapy, cargo transport, targeted drug delivery,[19,27] and recently on chemical sensors,[28] cell manipulation,[20] small pumps,[29] nanotools,[30] and microbullets[31] for bio-applications. Localized heat sensing is another interesting application, which holds great promise in biosensors (to monitor heat-producing bio-activities), lab on a chip, and micro/nano fluidics. In addition, in analogy to the "stop-and-go" or reversible operation of micro/nano motors through an external stimulus,[8,18,25,32] these tiny catalytic engines controlled by a focused laser beam are also

[a]*Department of Materials Science, Fudan University, Shanghai 200433, People's Republic of China. E-mail: yfm@fudan.edu.cn; Fax: +86-21-65643615; Tel: +86-21-65642829*

[b]*State Key Lab of ASIC and System, Fudan University, Shanghai 200433, People's Republic of China. E-mail: rliu@fudan.edu.cn*

† Electronic supplementary information (ESI) available. See DOI: 10.1039/c2nr32494f

capable of performing complex tasks on a micro/nano scale when incorporated with magnetic guidance.

In this work, we employed an external focused laser beam to perform local heat treatment on rolled-up catalytic engines and demonstrated the acceleration of propelled microtubes induced by laser heating. This photo-thermal effect provided the possibility of remote control of catalytic activities[33] in low concentrations of hydrogen peroxide through light. Furthermore, the external photo-thermal stimulus is capable of inducing still engines to expel bubbles in very low concentrations of chemical fuel (H_2O_2), making these chemically powered engines more biocompatible. It is also much easier to perform localized heating through the adjustment of the laser beam. The outcomes showed that the propulsion speed is linearly dependent on the laser power, indicating that the moving velocity of microengines increases with the temperature and therefore could be adopted to sense heat variation.

2 Experimental sections

In analogy to our previous works,[21,34,35] Ti/Cr/Pt microtubular engines were fabricated by e-beam evaporation onto substrates with lithographically patterned squares at an angle of 30° relative to the horizontal plane. The stressed tri-layers of 8 nm Ti, 8 nm Cr and 14 nm Pt were evaporated onto patterned substrates *via* electron beam under a high vacuum of 4.0×10^{-4} Pa at rates of 1 Å s^{-1}, 0.6 Å s^{-1}, and 0.3 Å s^{-1}, respectively. Due to the intrinsic strain in the layers, the deposited membranes rolled up into tubular structures after the selective removal of the underlying photoresist by ethanol. The fabricated tubes are 50–70 μm in length and have a uniform diameter of 12 μm. To activate the microengines, different concentrations of hydrogen peroxide were added as a fuel source to power the as-fabricated microtubes at room temperature. An optical microscope (Olympus BX51) with an integrated high-speed camera was adopted to capture the locomotion of the microengines at a rate of 30 frame s^{-1}. The velocities and trajectories were then analyzed with the help of a "Manual Tracking" plug-in in Image J.

An external laser in the wavelength of 650 nm with a fixed power of 80 mW was co-focused with the microscope on the focal plane (the heat spot diameter is around 350 μm) to observe the effect of localized heat treatment on the motion behaviour of the microengines, while a laser (wavelength 980 nm) with adjustable intensity was employed to illuminate the self-propelled microengines uniformly. The diameter of the near infrared laser spot (with wavelength of 980 nm) is around 0.8 cm, therefore the maximum power density reaches 2 W cm^{-2}.

3 Results and discussion

3.1 Microscale heating of catalytic microengines

Fig. 1a schematically presents the co-focus setup to perform localized laser heating from the interaction between the laser and the metallic layer, which increases the tube wall's temperature. A laser (wavelength 650 nm) with a fixed power of 80 mW was obliquely focused on the center of the focal plane by a lens. The diameter of the focused laser is around 350 μm. This setup enables us to freely observe the effect of a localized laser on self-propelled microengines or a single engine whilst simultaneously capturing live videos. The adjustment of the external laser also will not disturb the motion of catalytic microengines. The inset magnifies the region on the plane containing the moving engines in the focused laser spot and shows many autonomous microengines illuminated by laser. Fig. 1b displays the comparison of moving distances of a motor in circular motion before and after more than 35 s of localized heat treatment with a power density of ~8 W cm^{-2} (for details, see Video 1 in the ESI†). All the blue trajectories shown in this figure represent the moving path and distance in the same period of 600 ms. The left image in Fig. 1b shows the circular motion of a microengine in a concentration of ~4% v/v when the laser is off, the moving distance in 600 ms being around 370 μm, demonstrating an average speed of around 620 μm s^{-1}. After localized heat treatment to this single engine by a focused laser beam for more than 35 s, it takes less time to travel along the perimeter once. As can be seen in the right image in Fig. 1b, the moving distance Δs of the motor increased to about 540 μm in the same period. During the heating process, the laser spot has to be moved aside occasionally to capture the motion behavior of the microengine; otherwise strong reflected light from fast propelling bubbles will block the direct observation of micro engines since no filter lens was integrated into the microscope.

Circular motion is the typical motion behaviour of the catalytic microengines and was selected for detailed investigation. Due to the "meniscus-effect"[21] or "meniscus-climbing effect"[3] caused by capillary force at the air–liquid interface, the tubes attached themselves to the bubbles in a circle one by one and were simultaneously propelled by recoiling bubbles. These newly generated bubbles will keep tracing a circular path, giving rise to stable and sustained circular motion. Accidentally, during the local heating process, a complex motor comprising of multiple tubular engines entered into sight and linearly passed through the laser spot. The duration of laser heating to this complex motor is around 5 s. The comparison of moving distance Δs before and after passing through the laser spot can be seen in Fig. 1c (for details, see Video 1 in the ESI†). The increment of moving distance after ~5 s laser heating is about 70 μm in a period of 600 ms. Therefore, the speeds of both engines were enhanced by localized laser heating though the increment is not the same. The longer time of laser irradiation induces a larger speed enhancement, as can be seen in Fig. 1d. The increment shown in the left columns, representing circular motion velocity before and after more than 35 s of irradiation on circular motion, is more obvious than that of the right columns, representing the velocity enhancement after linearly passing through the laser spot. Thus, these microengines will not respond to laser heating immediately; both the heating process and the enhancement of moving speed need time.

3.2 Millimetre-scale heating of catalytic microengines

To study the effect of laser heating on the acceleration of catalytic engines and exclude the possibility that the speed

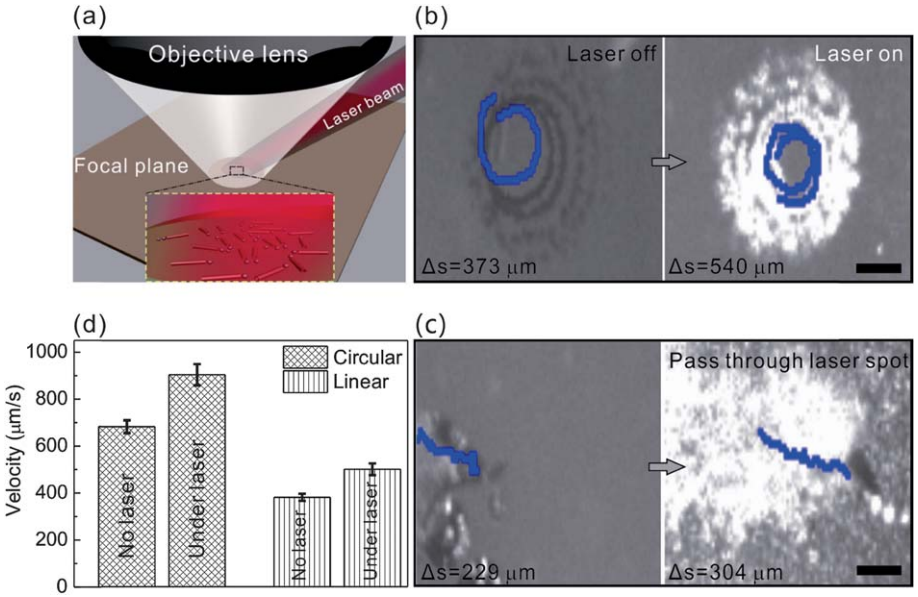

Fig. 1 (a) Schematic view of the co-focus setup for localized laser heat treatment on self-propelled catalytic microengines. Two different motions of microengines with respect to localized laser spots: (b) circular motion treated with localized laser for more than 35 s. Images show the circular motions without laser heating (left) and under laser heating. (c) Linear motion of microengine that just passed through the laser spot. Images show the linear motion without laser (left) and just passing through the laser spot (right). All blue trajectories represent the moving distances in 600 ms. (d) Diagram illustrating the corresponding speed enhancement of two microengines with circular motions (grid column) and linear motions (vertical lined column). All scale bars: 100 μm.

enhancement mentioned above is just a random case, a laser beam in the wavelength of 980 nm with maximum power density of 2 W cm^{-2} was adopted to simply illuminate the engines. The diameter of the laser spot is around 8 mm, which is much wider than that of the focused laser. Thus, the number of catalytic engines that can be irradiated greatly increased and collective motion acceleration upon laser irradiation would be more convincing. In the following demonstration, the laser in the wavelength of 980 nm was not focused by a lens and, instead, just illuminated the fuel tank containing the tiny engines.

As shown in Fig. 2a, after around an hour of catalytic reaction, large bubbles attracted each other by capillary force giving rise to bubble clusters at the air–liquid interface with inactive engines berthing on the border or becoming trapped inside. The low concentration of residual fuel is insufficient to make the engines escape from the bubbles. Before the laser is switched on, the entire "beach" is "peaceful" and the initial positions of four engines labelled (#1–4) are as displayed in Fig. 2a. After the laser is turned on, the engines are activated by laser heating, *i.e.* an increased temperature enables catalytic engines to work in a relatively low concentration of fuel.[14,24] The two engines in dashed circles in Fig. 2a come out once the laser is on, so the trajectories cannot be defined in this short time and these two engines can be just ignored. During laser irradiation, the engines trapped inside the bubble cluster (#5 and 6 with dashed arrow) entered into sight and overcame the capillary force to move freely. Microengine #7 was first pushed toward the bubble clusters by strong attracting capillary force between bubbles, and then induced by the high local temperature to escape from the bubble clusters. Fig. 2b is a frame extracted from the video exhibiting the situation after laser heating for around 15 s. Though near infrared laser cannot be seen by the naked eye, it can be sensed by the detector in a

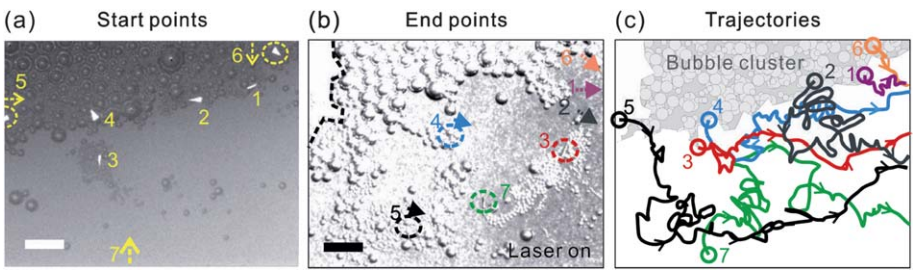

Fig. 2 (a) The image shows the tubular microengines (labelled as #1–7) initially berthed at the borders of bubble clusters without laser irradiation. During the laser irradiation, these microengines actively moved away from the bubble clusters in different trajectories, in which the final snap is shown in (b) and trajectories of the engines are recorded in (c). All scale bars: 200 μm.

high-speed camera, which is the reason why the image with laser irradiation is brighter.

Engines #1, 2, and 6 on the upper right corner in Fig. 2b have gone out of sight, while #3 and 7 are reactivated to run with fewer disturbances from bubbles and #4 is detaching from the cluster step by step. But #5 is still surrounded by bubbles and struggling to push attached bubbles away with the power supplied by laser heating (see Video 2 in ESI†). The area in the black dashed line in the upper left corner in Fig. 2b is another proof that catalytic engines are activated by laser irradiation in low fuel concentrations. The original bubbles in this area are either burst due to the accumulation of newly produced gas or pushed away by the activated engines. The trajectories of all these 7 engines are plotted in Fig. 2c, where small circles represent the initial positions in the bubble cluster and the arrows display the moving direction of activated engines. Almost all the trajectories that are not linear indicate the engine was tangled or trapped by bubbles; especially those suspended at the same place which were strongly attracted by capillary force. Eventually, all these engines were re-powered under laser irradiation and overcame the dragging force from the cluster. When the laser is switched off, tubular engines will be pulled back in a short time and detach from the cluster again after turning on the laser. This attaching and detaching process *via* laser control is reproducible and repeatable. In addition, this collective and reproducible response of catalytic microengines to laser irradiation indicates the heat modulation of laser irradiation and thus the potential strategy to photo-thermally control the motion of microengines by laser.

3.3 Lowering the limit of fuel concentration

Fig. 3 exhibits the effect of laser heating on an individual inactive tubular engine. At the end of catalytic reaction, the engines almost cannot be powered to move when the concentration of chemical fuel is much lower than 1.5% v/v, which is the lowest concentration for propelling rolled-up microengines in our case. In Fig. 3a an imperfectly rolled up microengine is floating in the solution, and when the laser is switched on for a while this engine starts to generate bubbles but at a low generation frequency, as shown in Fig. 3b. But in the video (see the Video 3 in the ESI†) bubbles are sequentially ejected from both ends, analogues to the "overloaded pumps" demonstrated in the literature,[29] possibly caused by this complex structure. The low bubble generation frequency may be another cause of dual bubble propulsion because the dynamic provided by this inefficient propulsion is not adequate to activate the motion, giving rise to the diffusion of fuel from both ends and thus to dual bubble generation. We studied the dependence of bubble generation frequency of this engine on the time of laser irradiation, as displayed in the diagram in Fig. 3c. The response of bubble generation is not so immediate when the laser is switched on, as shown in the red arrow. After 4.5 s of laser irradiation the still engine starts to propel bubbles from both ends and the bubble generation frequency (bubbles generated from both ends per second) rises within the duration of laser heating. When the laser is switched off, the propelling of bubbles gradually ceases and the speed of the engine returns to zero (see in the Video 3 in the ESI†).

This effect may be mainly attributed to the heating of the metallic microengines. Simultaneously, the photons can interact with electrons in the curved metallic film, exciting surface plasmons or causing collective electron oscillation in the metallic nanostructures[36–39] and thus generating heat by Landau damping in metals[39] to enhance the chemical reaction in a nearby medium.[24] Another point of view to explain the effect is through photon-enhanced chemical reaction.[40] Electrons excited by laser irradiation or elevated temperature induced by laser heating could improve the catalytic rate and promote bubble generation in low fuel concentrations.[24] Generally, in this case it can be concluded that laser irradiation can enhance the catalytic decomposition of hydrogen peroxide and lower the threshold concentration of chemical fuel needed to propel rolled-up metallic engines. More significantly, it is also possible to perform much more complex tasks by combining the speed regulation under laser irradiation with direction control by magnetic guidance.

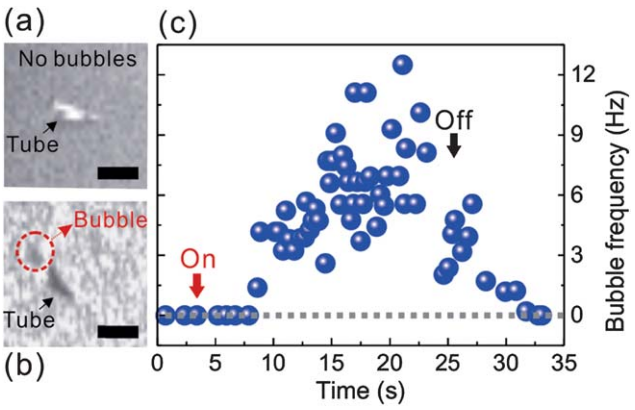

Fig. 3 (a) Optical image showing an inactive microtubular engine with no bubbles generated under a low concentration of fuel. Once illuminated under a laser, the engine starts to generate bubbles. Shown in (b) is the optical image with laser on for 4.5 s. (c) The graph presents the dependence of bubble generation frequency on the irradiation time of the laser, in which the "On" and "Off" refers to laser on and off. All scale bars: 50 μm.

3.4 On/off heat sensing

To study the effect of laser illumination on the speed enhancement of individual moving engines in a low concentration of 2% v/v, the trajectories of three engines before and after laser irradiation with maximum power were recorded and displayed in Fig. 4 (see the Video 4 in the ESI†). All the blue lines represent the moving route in the same period of 1.5 s. Without any external stimulus the moving distances Δs of three microengines are 667, 303, and 544 μm, respectively, and the corresponding average velocities are 445, 202, and 362 μm s^{-1}, as shown in Fig. 4a–c. After irradiation of around 20 s when the motion of these three engines is enhanced and stable, the moving distances Δs, correspondingly, increase to 862, 941, and 758 μm in 1.5 s, thus the average velocities have raised to 575, 628, and 505 μm s^{-1} respectively. Generally, the microengines

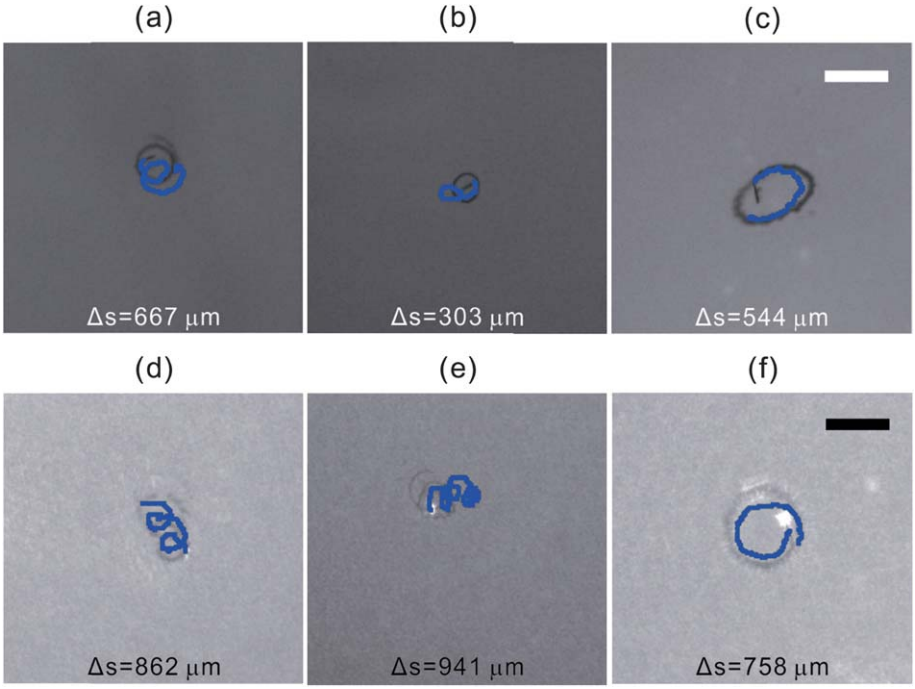

Fig. 4 Motion trajectories of three individual microengines in ~2% H_2O_2 solution are shown in (a)–(c). After ~20 s of laser irradiation, the corresponding trajectories are shown in (d), (e), and (f), respectively. All the trajectories were recorded in the same period of 1.5 s. All scale bars: 200 μm.

that have been irradiated for a certain time will speed up, with the increment percentage ranging from 29.3% to 200%. The wide range may be caused by external factors like the non-uniform distribution of laser intensity, bubble bursting, as well as environmental vibration during operation, which may also disturb the motion speed and further cause the deviation between the blue trajectories and bubble tails as shown in Fig. 4a, b and e. However, the speeds of these three irradiated targets are indeed improved. This photo-thermal effect raises the temperature in the illuminated region near to targeted engines, stimulating catalytic decomposition of hydrogen peroxide to oxygen bubbles and thus enhancing the speed. Simultaneously, an elevated temperature will decrease the viscosity of the fuel solution,[24] giving rise to less resistance in the local heated area.

To perform delicate tasks in fluidics, simple acceleration of individual engines is not sufficient and thus modulation of motion speed by laser irradiation is required. Therefore, in Fig. 5, the velocity of an identical engine regulated by laser heating is recorded and calculated as a function of time of irradiation (for details, see the Video 5 in the ESI†). For convenient prolonged monitoring of single engines, stable and slow motion in low concentrations is needed. The concentration of H_2O_2 we used here is 2% v/v. Precise and consecutive velocity distribution was difficult to obtain due to interruption by external manual operation to track the moving target. Every calculated dot in the diagram is based on the stable captured videos. The red curve (representing laser **on**) and dashed grey one (meaning laser **off**) show the tendency of speed variations when switching the laser on/off. As we can see, the speed of one laser-accelerated engine diminishes when the laser is switched off, as exhibited by the first grey dashed curve in Fig. 5. After switching the laser on again, the velocity of this engine is accelerated to the initial peak value in around one minute. Therefore, it can be speculated that this photo-thermal control of microengines can be repeated continuously and reversibly until the fuel is depleted. It also provides a possible method to regulate the motion speed by controlling the time of laser irradiation, which can also be proved by the velocity comparison between one tubular engine treated with prolonged focused heat treatment and the other complex one that happened to pass through laser spot in Fig. 1.

3.5 Dependence of heat power on motion velocity

As a heat sensor, the velocity of catalytic engines was adopted to sense the temperature variation. Thus it is necessary to study

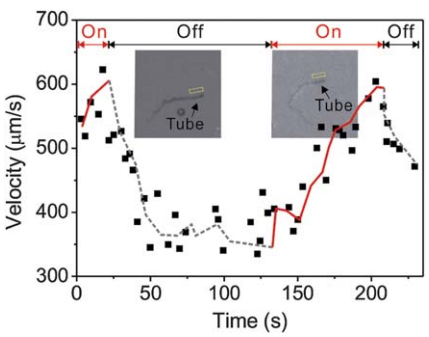

Fig. 5 Graph displays the velocity modulation of a tubular microengine as a function of time when laser is ON and OFF. The insets show the same tube when laser is off (left) and on (right).

the dependence of catalytic propulsion on temperature. Herein, we studied the velocity variation as a function of laser power intensity instead of local temperature as presented in Fig. 6d. The average velocity in this diagram is calculated after analyzing 3 tubes in the same condition over the same period. Taking the single engine in a concentration of ~10% v/v hydrogen peroxide as an example, the moving distance of this tube in a time interval of 900 ms was captured when the laser is shut down (power 0) as shown in Fig. 6a. After tuning the laser power density to 1000 mW cm^{-2} and illuminating the engine for 2.5 min, the moving distance increases to 793 μm in the same period. It takes some time ranging from several seconds to several minutes to heat up the solution as displayed in the discussion of Fig. 3 and illustrated in the previous literature,[36] therefore the time of irradiation is prolonged to saturate and stabilize the motion speed before capturing the video for velocity calculation. The depletion of fuel in this case may have some effect on the increment of motion velocity for the enhanced and time-consuming propulsion process. But the speed of this engine is further accelerated after laser illumination with maximum power (2000 mW cm^{-2}) for another 2.5 min, as can be seen in Fig. 6c, where the moving distance rises up to about 1 mm in 900 ms. In the concentration of 10% v/v H_2O_2 the velocity increases linearly with the laser power density (corresponding to the local temperature around the microengines), indicating a potential candidate for heat sensor application.

Following the same procedures, the average velocities of three engines in 5% v/v H_2O_2 after laser irradiation with different power densities were calculated and compared with the ones in 10% v/v H_2O_2, as depicted in Fig. 6d. Both curves follow a linear trend, which well agrees with previous reports[24] when the laser heat treatment starts from room temperature (>20 °C). It is also worth noting that the velocity increment irradiated by maximum power in 5% v/v H_2O_2 is not as large as the one in 10% v/v H_2O_2, comparing the slope of the two lines. The speed enhancement may be limited by the consumption of fuel as well as an inadequate energy supply under low concentrations of fuel and low laser power (temperature). When the fuel is sufficient, external stimuli will dominate the motion control; however, the concentration of fuel will be the limitation to reach the expected response to a strong external stimulus.

Therefore, another promising approach to control motion speed by tuning local temperature is to adjust the power density of the focused laser. To modulate the motion speed of microengines, versatile methods can be developed to control the local conditions on the foundation of a focused laser, *e.g.* irradiation time, location of laser spot, and laser power. Though most of the investigation in this work was simply illuminated by a laser with 0.8 cm spot diameter, it can be speculated that the laser induced heating effect can also work for a focused laser. Moreover, a focused laser can be readily obtained and integrated with other equipment in future applications, especially those on a micro/nano scale.

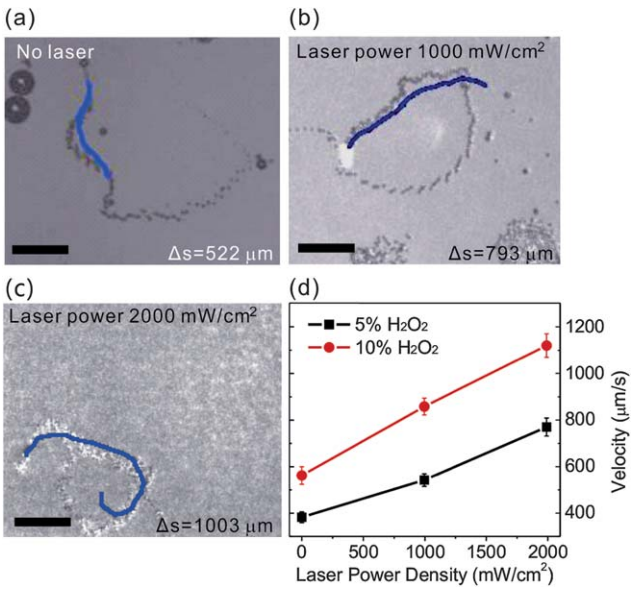

Fig. 6 Optical images show a self-propelled microengine in ~10% H_2O_2 (a) without laser irradiation, (b) under laser irradiation with a power of 1000 mW cm^{-2}, and (c) 2000 mW cm^{-2} (c), respectively. All trajectories were recorded within 900 ms. All scale bars are 200 μm. (d) Graph presents the relationship between motion velocity of the engines and laser power in different fuel concentrations (black squares: 5% and red dots: 10%).

4 Conclusions

In conclusion, we have successfully demonstrated the acceleration effect of a focused laser on engine propulsion in different concentrations of fuel. The laser induced heating effect can elevate the local temperature and thus photo-thermally accelerate or modulate the motion speed of catalytic rolled-up microengines. This photo-thermal effect also lowers the threshold concentration of fuel (here H_2O_2) to propel the tube, which is of great importance for future applications. Focused lasers can also be more widely used in future micro/nano applications. By adjusting the laser parameters such as irradiation time and power, the moving velocity of engines can be accelerated and even regulated. In the power range of laser used in this work, the speed increases linearly with the power irradiated on the nearby medium. Such linear trends displayed by the velocity/local temperature dependence indicate promising applications for these tiny catalytic rolled-up microengines as a small-scale heat sensor. This work offers a novel approach to modulating the motion of metallic rolled-up microengines in low concentrations of H_2O_2, as well as a potential micro-scale heat detector. Future exploration of such functions could enable catalytic micro/nano motors to fulfil more complex tasks in smart drug delivery, lab-on-a-chip applications and so on.[5]

Acknowledgements

This work is supported by "Shu Guang" project by Shanghai Municipal Education Commission and Shanghai Education Development Foundation and the Natural Science Foundation of China (nos 61008029 and 51102049). RL thanks the support

from the National High Technology Program (2011AA100706-2) and the National Science Foundation of China (61171010).

Notes and references

1 R. F. Ismagilov, A. Schwartz, N. Bowden and G. M. Whitesides, Autonomous movement and self-assembly, *Angew. Chem., Int. Ed.*, 2002, **41**, 652.
2 A. A. Solovev, Y. F. Mei, E. Bermúdez Ureña, G. S. Huang and O. G. Schmidt, Catalytic microtubular jet engines self-propelled by accumulated gas bubbles, *Small*, 2009, **5**, 1688–1692.
3 A. A. Solovev, Y. F. Mei and O. G. Schmidt, Catalytic microstrider at the air–liquid interface, *Adv. Mater.*, 2010, **22**, 4340.
4 A. A. Solovev, S. Sanchez, M. Pumera, Y. F. Mei and O. G. Schmidt, Magnetic control of tubular catalytic microbots for the transport, assembly, and delivery of micro-objects, *Adv. Funct. Mater.*, 2010, **20**, 2430.
5 Y. F. Mei, A. A. Solovev, S. Sanchez and O. G. Schmidt, Rolled-up nanotech on polymers: from basic perception to self-propelled catalytic microengines, *Chem. Soc. Rev.*, 2011, **40**, 2109.
6 Y. F. Mei, G. S. Huang, A. A. Solovev, E. B. Urena, I. Moench, F. Ding, T. Reindl, R. K. Y. Fu, P. K. Chu and O. G. Schmidt, Versatile approach for integrative and functionalized tubes by strain engineering of nanomembranes on polymers, *Adv. Mater.*, 2008, **20**, 4085.
7 W. Gao, A. Uygun and J. Wang, Hydrogen-bubble-propelled zinc-based microrockets in strongly acidic media, *J. Am. Chem. Soc.*, 2012, **134**, 897.
8 J. Burdick, R. Laocharoensuk, P. M. Wheat, J. D. Posner and J. Wang, Synthetic nanomotors in microchannel networks: directional microchip motion and controlled manipulation of cargo, *J. Am. Chem. Soc.*, 2008, **130**, 8164.
9 J. G. Gibbs, N. A. Fragnito and Y. P. Zhao, Asymmetric Pt/Au coated catalytic micromotors fabricated by dynamic shadowing growth, *Appl. Phys. Lett.*, 2010, **97**, 253107.
10 J. G. Gibbs and Y. P. Zhao, Self-organized multiconstituent catalytic nanomotors, *Small*, 2010, **6**, 1656.
11 K. M. Manesh, S. Balasubramanian and J. Wang, Nanomotor-based 'writing' of surface microstructures, *Chem. Commun.*, 2010, **46**, 5704.
12 M. Pumera, Electrochemically powered self-propelled electrophoretic nanosubmarines, *Nanoscale*, 2010, **2**, 1643–1649.
13 P. M. Wheat, N. A. Marine, J. L. Moran and J. D. Posner, Rapid fabrication of bimetallic spherical motors, *Langmuir*, 2010, **26**, 13052.
14 S. Balasubramanian, D. Kagan, K. M. Manesh, P. Calvo-Marzal, G.-U. Flechsig and J. Wang, Thermal modulation of nanomotor movement, *Small*, 2009, **5**, 1569.
15 W. Gao, S. Sattayasamitsathit, J. Orozco and J. Wang, Highly efficient catalytic microengines: template electrosynthesis of polyaniline/platinum microtubes, *J. Am. Chem. Soc.*, 2011, **133**, 11862.
16 K. M. Manesh, M. Cardona, R. Yuan, M. Clark, D. Kagan, S. Balasubramanian and J. Wang, Template-assisted fabrication of salt-independent catalytic tubular microengines, *ACS Nano*, 2010, **4**, 1799.
17 W. Gao, S. Sattayasamitsathit, A. Uygun, A. Pei, A. Ponedal and J. Wang, Polymer-based tubular microbots: role of composition and preparation, *Nanoscale*, 2012, **4**, 2447.
18 J. Wang and K. M. Manesh, Motion control at the nanoscale, *Small*, 2010, **6**, 338.
19 G. S. Huang, J. Wang and Y. Mei, Material considerations and locomotive capability in catalytic tubular microengines, *J. Mater. Chem.*, 2012, **22**, 6519.
20 S. Sanchez, A. A. Solovev, S. Schulze and O. G. Schmidt, Controlled manipulation of multiple cells using catalytic microbots, *Chem. Commun.*, 2011, **47**, 698.
21 J. X. Li, B. R. Lu, Z. K. Shen, Z. C. Xu, H. Li, J. J. Wen, Z. D. Li, X. P. Qu, Y. F. Chen, Y. F. Mei and R. Liu, Magnetic and meniscus-effect control of catalytic rolled-up micromotors, *Microelectron. Eng.*, 2011, **88**, 1792.
22 W. Gao, S. Sattayasamitsathit and J. Wang, Catalytically propelled micro-/nanomotors: how fast can they move?, *Chem. Rec.*, 2012, **12**, 224.
23 P. Calvo-Marzal, K. M. Manesh, D. Kagan, S. Balasubramanian, M. Cardona, G.-U. Flechsig, J. Posner and J. Wang, Electrochemically-triggered motion of catalytic nanomotors, *Chem. Commun.*, 2009, 4509.
24 S. Sanchez, A. N. Ananth, V. M. Fomin, M. Viehrig and O. G. Schmidt, Superfast motion of catalytic microjet engines at physiological temperature, *J. Am. Chem. Soc.*, 2011, **133**, 14860.
25 A. A. Solovev, E. J. Smith, C. C. Bof 'Bufon, S. Sanchez and O. G. Schmidt, Light-controlled propulsion of catalytic microengines, *Angew. Chem., Int. Ed.*, 2011, **50**, 10875.
26 M. Ibele, T. E. Mallouk and A. Sen, Schooling behavior of light-powered autonomous micromotors in water, *Angew. Chem., Int. Ed.*, 2009, **48**, 3308.
27 J. Wang and W. Gao, Nano/microscale motors: biomedical opportunities and challenges, *ACS Nano*, 2012, **6**, 5745.
28 D. Kagan, P. Calvo-Marzal, S. Balasubramanian, S. Sattayasamitsathit, K. M. Manesh, G. U. Flechsig and J. Wang, Chemical sensing based on catalytic nanomotors: motion-based detection of trace silver, *J. Am. Chem. Soc.*, 2009, **131**, 12082.
29 A. A. Solovev, S. Sanchez, Y. F. Mei and O. G. Schmidt, Tunable catalytic tubular micro-pumps operating at low concentrations of hydrogen peroxide, *Phys. Chem. Chem. Phys.*, 2011, **13**, 10131.
30 A. A. Solovev, W. Xi, D. H. Gracias, S. M. Harazim, C. Deneke, S. Sanchez and O. G. Schmidt, Self-propelled nanotools, *ACS Nano*, 2012, **6**, 1751.
31 D. Kagan, M. J. Benchimol, J. C. Claussen, E. Chuluun-Erdene, S. Esener and J. Wang, Acoustic droplet vaporization and propulsion of perfluorocarbon-loaded microbullets for targeted tissue penetration and deformation, *Angew. Chem., Int. Ed.*, 2012, **51**, 7519.

32 W. Gao, S. Sattayasamitsathit, K. M. Manesh, D. Weihs and J. Wang, Magnetically powered flexible metal nanowire motors, *J. Am. Chem. Soc.*, 2010, **132**, 14403.
33 B. M. Neilson and C. W. Bielawski, Photoswitchable organocatalysis: using light to modulate the catalytic activities of *N*-heterocyclic carbenes, *J. Am. Chem. Soc.*, 2012, **134**, 12693.
34 J. X. Li, G. S. Huang, M. M. Ye, M. L. Li, R. Liu and Y. F. Mei, Dynamics of catalytic tubular microjet engines: dependence on geometry and chemical environment, *Nanoscale*, 2011, **3**, 5083.
35 W. M. Li, G. S. Huang, J. Wang, Y. Yu, X. J. Wu, X. G. Cui and Y. F. Mei, Superelastic metal microsprings as fluidic sensors and actuators, *Lab Chip*, 2012, **12**, 2322.
36 V. Abdelsayed, S. Moussa, H. M. Hassan, H. S. Aluri, M. M. Collinson and M. S. El-Shall, Photothermal deoxygenation of graphite oxide with laser excitation in solution and graphene-aided increase in water temperature, *J. Phys. Chem. Lett.*, 2010, **1**, 2804.
37 D. Werner, S. Hashimoto and T. Uwada, Remarkable photothermal effect of interband excitation on nanosecond laser-induced reshaping and size reduction of pseudospherical gold nanoparticles in aqueous solution, *Langmuir*, 2010, **26**, 9956.
38 X. Huang, S. Tang, X. Mu, Y. Dai, G. Chen, Z. Zhou, F. Ruan, Z. Yang and N. Zheng, Freestanding palladium nanosheets with plasmonic and catalytic properties, *Nat. Nanotechnol.*, 2011, **6**, 28.
39 L. Cao, D. N. Barsic, A. R. Guichard and M. L. Brongersma, Plasmon-assisted local temperature control to pattern individual semiconductor nanowires and carbon nanotubes, *Nano Lett.*, 2007, **7**, 3523.
40 A. Nitzan and L. E. Brus, Theoretical-model for Enhanced Photochemistry on Rough Surfaces, *J. Chem. Phys.*, 1981, **75**, 2205.

